OKU Fen Bilimleri Enstitüsü Dergisi
5(3): 1244-1273, 2022

OKU Journal of The Institute of Science and Technology, 5(3): 1244-1273, 2022.

Osmaniye Korkut Ata Üniversitesi Fen Bilimleri Enstitüsü Dergisi

Osmaniye Korkut Ata University Journal of The Institute of Science and Technology

Fotovoltaik Sistemlerde İzleme Algoritması İçin Yeni Bir Uygulama Yaklaşımı

Mustafa HASAN[1*], Serra ALTINOLUK[1,2]

[1]Muğla Sıtkı Koçman Üniversitesi/Electrical & Electronics Engineering, Muğla, Turkey
[2]The Center for Solar Energy Research and Applications (GÜNAM), Ankara, Turkey

[1]https://orcid.org/0000-0003-2325-4815
[2]https://orcid.org/ 0000-0003-4347-3804
*Sorumlu yazar: eng.mustafa.lateef@gmail.com

Araştırma Makalesi

Makale Tarihçesi:
Geliş tarihi: 20.02.2022
Kabul tarihi:23.05.2022
Online Yayınlanma: 12.12.2022

Anahtar Kelimeler:
PV sistem
Buck dönüştürücü
PI kontrolör
PIC18F4580
MSX-60
Eşleştirme

ÖZ

Bu makalede, mikrodenetleyicilerle ilgilenen devre simülasyonlarının çoğunda güneş pili modüllerinin eksikliğinin üstesinden gelmek için yeni bir modelleme tekniği anlatılmaktadır. Önerilen yeni uygulama, en popüler platformlardan biri olan Proteus ve MikroC yazılımına dayanmaktadır. Gerçeğe yakın emülasyon yapmak için, sıcaklık ve insidans ışınımı değiştirme olasılığı dahilinde MSX-60 panelini matematiksel denklemlere dayalı olarak simülasyonu amaçlanmaktadır. Sunulan çalışma, IV ve PV karakteristiğini veri sayfası tarafından sağlanan çıktılar ile karşılaştırarak önerilen sistemin geçerliliğini test etmenin yanı sıra, bir değişken girişten oluşan sistem üzerinde, PIC18F4580 mikro denetleyici tarafından izleme voltajı algoritması uygulamak için yeni bir teknik önermektedir. Kaynak PV sistemi, bir ara madde olarak bir güç elektroniği cihazının önceden varlığı ile bir yükü beslemektedir. Buck dönüştürücü, istenen çıkış voltajını takip etmekle aynı anda düzensizlik durumunda en iyi performansa erişmek için bu kısmı kullanmaktadır. Ayrıntılı ayrık PI algoritması uygulama süreci ve burada sunulan diğer ilişkili aksesuarlarla eşleme tekniği, başka yerlerde nadiren kullanılmaktadır. Simülasyon sonuçları, hem ışınım hem de sıcaklık arasındaki ilişkiyi voltajla doğrulayarak önerilen modellemenin geçerliliğini kanıtlamıştır. Buck dönüştürücünün kapalı çevrim kontrol sisteminde, önerilen sistemin tümü, ortam sıcaklığı ve ışınlamanın değişmesinden bağımsız olarak, voltaj izleme ve istenen voltajın takibi konusunda mükemmel bir yanıt göstermiştir.

A New Implementing Approach for Tracking Algorithm on Photovoltaic Systems

Research Article

Article History:
Received: 20.02.2022
Accepted: 23.05.2022
Published online: 12.12.2022

Keywords:
PV system
Buck converter
PI controller
PIC18F4580
MSX-60
Mapping

ABSTRACT

This paper introduces a modelling technique to overcome the lack of solar cell modules in most of the circuit simulations that deals with the microcontrollers. The new implementation is based on Proteus, which is one of the most popular platforms, and MikroC software. For emulation close to reality, it aims to simulate the MSX-60 panel based on mathematical equations within the possibility of varying the temperature and the incidence irradiation. In addition to testing the validity of the proposed system by comparing the IV and PV characteristics with the outputs provided by the data sheet, the presented study proposes a new technique to implement a tracking voltage algorithm by the PIC18F4580 microcontroller on a variable input system. The source PV system feeds a load with the prior presence of a power electronic device as an intermediate. The buck converter uses this part to simultaneously follow the desired output voltage and achieve the best performance in case of disturbance. The detailed discrete PI algorithm

implementing process and the mapping technique with the other associated accessories presented here are rarely used elsewhere. Simulation results proved the validity of the proposed modelling by confirming the relationship between both the irradiation and temperature with voltage. In the closed-loop control system of the buck converter, the proposed system all showed a perfect response regarding the voltage tracking and chasing the desired voltage irrespective of varying the ambient temperature and the irradiation.

To Cite: Hasan M., Altınoluk S. A New Implementing Approach for Tracking Algorithm on Photovoltaic Systems. Osmaniye Korkut Ata Üniversitesi Fen Bilimleri Enstitüsü Dergisi 2022; 5(3): 1244-1273.

1. Introduction

Renewable energy's usage has been restrained by human innovation. It has been harnessed since ancient times via various technologies. In addition to the adverse impact of the use of conventional methods, exponentially ascending of energy demand are the main reasons for the global warming crisis that in some way pushing the whole world toward the brinkmanship (Ayim et al., 2019). These facts emphasize the need for us to explore additional sustainable energy resources for saving our planet (Çiftçi et al., 2020). In this regard, one of the promising ways is investment in solar energy, which is one of the cleanest and free recourses in nature (Bulut et al., 2018). Being able to convert solar energy into electrical energy will solve the energy demand problem.

The photovoltaic (PV) system converts the incident sunlight beam directly into electrical energy. The PV system is based on solar cells, and these cells are connected in either parallel or series manner for forming a PV module that is further being connected together in a specific style to form a PV array. According to the desired voltage and the application requirements, PV connections can end up as either array or module. The reason for that is the higher electrical energy production will occur by increasing the area of the PV array or module interacting with the sunlight. The P-V and V-I PV system characteristics can be deduced by the characteristic equation of the single diode equivalent circuit of the PV system (Orioli, 2020).

Although free energy source based PV applications innated on PV cells are very attractive, the shortage of accurate voltage control beside the wasted energy can be the troublesome part of this technology. From this point of view, one of the proposed techniques to overcome this dilemma is connecting a power electronic device intermediately between the PV cell and the load. This device will adjust the output voltage and reduce the power loss (Loba and Salim, 2013; Kandilli, 2017; Pal et al., 2017; Zhou and Macaulay, 2017).

In general, the efficiency of a PV cell depends on the manufacturing materials and the utilized control mechanisms.

The amount of benefiting from the sun will be different at different times of the day (e.g., night and day, irradiation, ambient temperature). For that reason the user expects from the solar cell handing the different amount of power around a day. In this regard, the Maximum Power Point Tracking (MPPT) technique used to extract maximum allowable power from the solar cell irrespective of environmental conditions (this theme beyond the aim of this work).

As stated in our previous work, PV ambient temperature and irradiation amounts are the factors having the most effective impact on the output characteristics of a PV cell (Mustafa et al., 2020). Increasing temperature has a negative effect on the system, but for irradiation just vice versa (Wang et al., 2021). For that reason, in specific applications that need to operate or run at a certain voltage, regardless of the output disturbance, there must be a power electronic device to compensate the change.

In solar panels, one of the proposed techniques to regulate the output voltage is using a buck converter. It is a power electronic device used for diminishing the input voltage to a range from 0 up to the input voltage via manipulating the duty cycle (Rashid, 2011). The microcontroller is used to generate and control the frequency and the duty cycle value of the Pulse-Width Modulation (PWM) signal. To validate the efficiency and the performance of such a system, the PV panel needs to be modelled. To achieve this an intensive effort has been done by researchers and companies. Nowadays MATLAB/Simulink and other related simulation softwares had included the PV model (Erdoğan et al., 2014; Motahhr et al., 2015; Akcan et al, 2020); nevertheless, these tools suffer from a shortage of existing electronic board or a microcontroller in which our proposed technique would be tested or implemented. Consequently, for our work, these kind of platforms are neither trusted, nor suitable for validating the proposed algorithm.

Despite all of the evolution and progress that PV cells developed in terms of fabrication and manufacturing, it does not exist as a device or a component in most circuit simulation platforms. To overcome this lack and shortage, we designed a prototype to emulate this shortfall and fill the gap in this aspect.

One of the most popular tools to deal with the existence of microcontrollers and electronic boards is Proteus. To make sure that Proteus is keeping pace with PV technological developments, (Motahhir et al., 2017) the authors designed a PV system based on a mathematical equation of a single diode equivalent circuit regardless of the temperature and irradiation, and other weather conditions changes during the day. In literature, double diode model was also used, instead of one (Yaqoob and Obed, 2020).

In (Chalh et al., 2020) work, they went beyond that and they tested it with MPPT. If more detailed examinatin is done, it can be deduced that none of them has taken into consideration to simulate the case of the temperature or irradiation change on a fully connected system. The researchers preferred changing the SPICE code for the diode, which can be assumed to be relatively easier.

To address this deficiency, we developed a prototype system that would simulate the case of adjusting the system operating conditions, irradiation, and temperature. Then our model is validated by comparing the outcome data of PV characteristic with experimental one provided by the MSX-60 PV datasheet. The second part of our work includes the derivation and implementation of a unique digital PI algorithm applicable in the microcontroller unit; used to keep the output voltage of a designed buck converter working at a constant voltage irrespective of varying the ambient temperature or the irradiance.

2. Materials and Method

The process flow chart of the research study and the components of the system are illustrated in Figure 1 and in Figure 2 respectively. The system consists of: i) PV cell with parameters provided at the manufacturing datasheet, ii) step down converter, iii) feedback to sense the output voltage and fed it back to the proposed controller to obtain constant output voltage at the load irrespective of the variation in solar irradiance and temperature, iv) resistive load, v) Proportional-Integral controller, and vi) Keypad for opting the desirable input voltage. The proposed schematic is developed using Proteus 8,9. Meanwhile, the MikroC platform is used as a base for implementing the real-time microcontroller. The mapping process acts as an intermediate part between adjacent inconsistent parts. In other words, it is used for scaling the output values of the first block to another range. The voltage divider is used to protect the microcontroller from burning due to excessive voltage and achieving the mapping process on the output value of the digital PI controller converting it to another scale. The voltage applied on DC load is fed back to the digital controller through a voltage divider for aforementioned reasons, besides, to compare it with the desired voltage. The result represents the error which is used as the base for producing the duty cycle value driving the MOSFET of the buck converter.

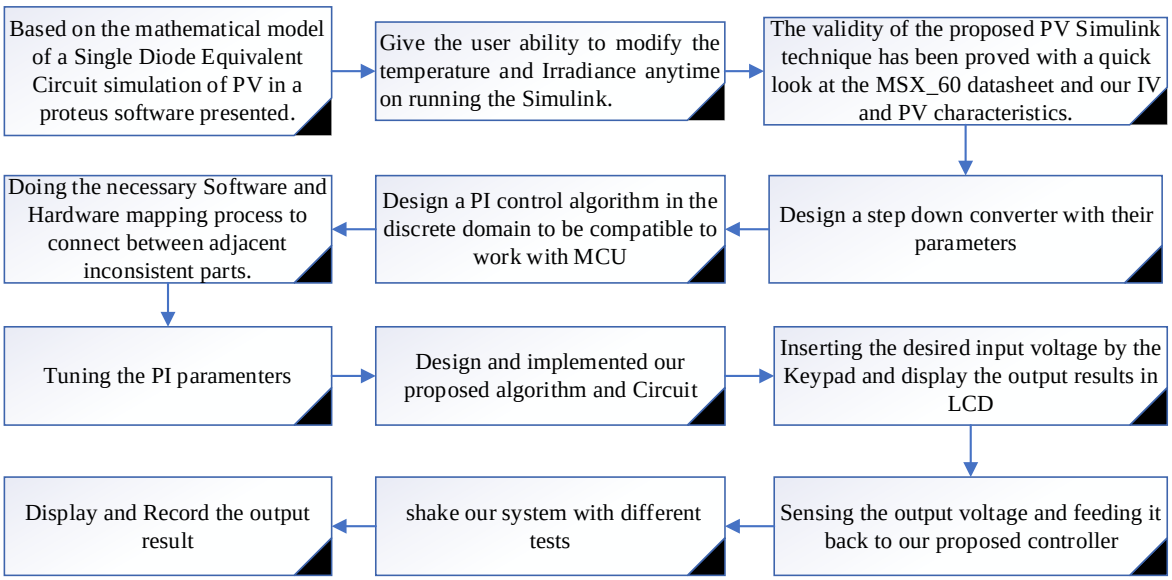

Figure 1. The flow diagram of the study.

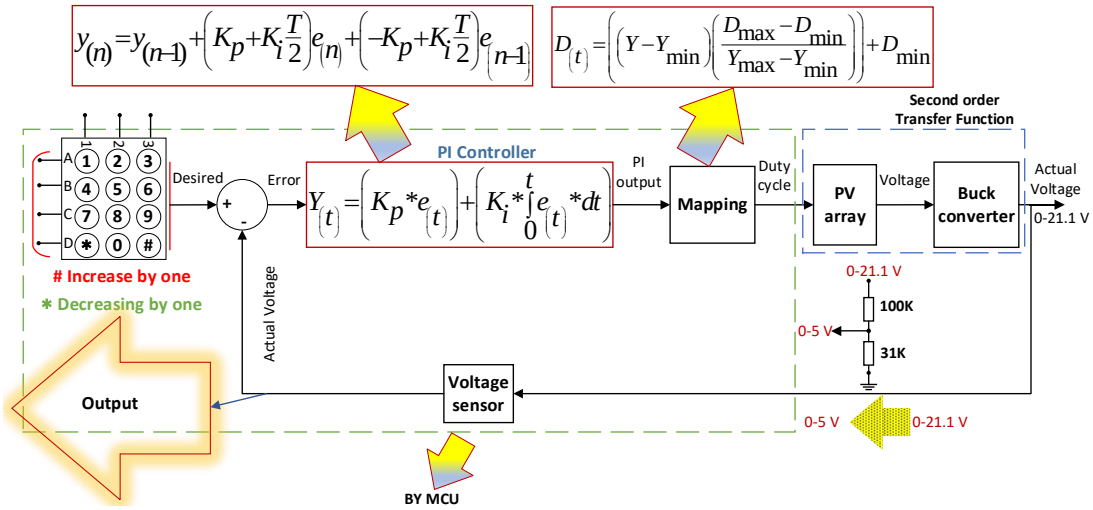

Figure 2. The proposed system for controlling the output voltage by PIC18F4580.

The solar PV module is the main voltage source feeding the DC load with a constant voltage through the buck converter. PIC18F4580 plays a pivotal role in these processes: starting from selecting the desired voltage and so on, and ending up to produce the PWM signal. The PIC18F4580 roles in this algorithm are:

- Playing a pivotal role during selection of the desired voltage in the Keypad and modifying while the system is running.
- Sensing the actual output voltage via the help of ADC registers and feeding it back to subtract it from the desirable one.
- Since we are dealing with MCU in the tracking algorithm part, in other words, we have to deal with the discrete domain. So, after deriving the applicable PI discrete domain in MCU, the calculated error entering that discrete equation forming PI output.
- The PI output values need to be scaled or mapped to another specific range; the MCU is responsible for that part.
- Finally, with MCU help CCP produces the PWM signal at a specific frequency and controls the output duty cycle. The PWM signal uses to keep the system operate as the user desires. In addition to that, the MCU is responsible for the LCD, showing the output voltage value, the desired one, and the duty cycle value.

2.1. Solar cell modelling and simulation

Providing an accurate mathematical model is a crucial step to simulate the circuit of the solar cell. According to (Zekry et al., 2018) the below equations summarize the mathematical equations that describe the solar cell in the single-diode model form as depicted in Figure 3. It consists of a current source in parallel with one diode beside shunt and series resistors (Luque and Hegedus, 2011).

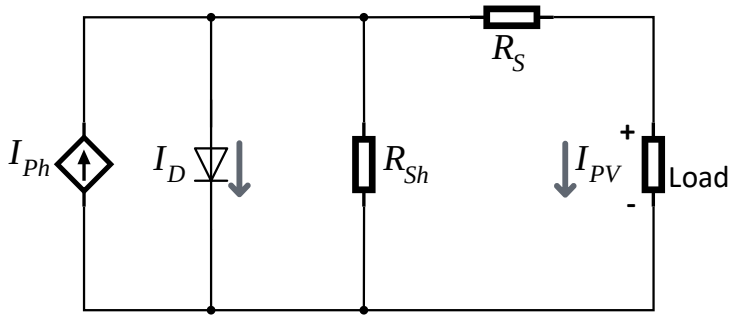

Figure 3. Equivalent circuit of PV cell.

$$I_{Ph} = \frac{G}{G_{(STC)}} I_{SC(STC)} + [(T - T_{STC})K_i] \quad (1)$$

$$I_{s(STC)} = \frac{I_{SC(STC)}}{e^{\frac{q*V_{OC(STC)}}{K_B*T_{STC}*N_s*n}} - 1} \quad (2)$$

$$I_s = I_{s(STC)} \left(\frac{T}{T_{STC}}\right)^3 * e^{\frac{-qE_g\left(\frac{1}{T} - \frac{1}{T_{STC}}\right)}{n*K_B}} \quad (3)$$

$$I_D = \left(e^{\frac{q(V+I_{Pv}R_S)}{K_B*T*N_s*n}} - 1\right) * I_s * N_p \quad (4)$$

$$I_{sh} = \frac{V+IR_s}{R_{sh}} \quad (5)$$

$$I_{Pv} = I_{Ph} - I_D - I_{sh} \quad (6)$$

$$V_{OC} = V_{OC(STC)} + [(T - T_{STC})K_v] \quad (7)$$

The solar cell precise modelling is based on the accurate parameters' extraction in that model. These parameters are I_{Ph}, I_s, R_s , R_{sh}, and n. In our work, the Solarex MSX-60 panel modelling is based on (EL Tayyan, 2013) extraction work and the datasheet of the manufacturer's specifications which are given in Standard Test Conditions (STC).

$$I_{Ph} = G * 3{,}8m + [(T - 298)2{,}4m] \quad (8)$$

Scaling the voltage from a range 0 to 5 V to yield the irradiation in range 200 to 1000 $\frac{w}{m^2}$ done by $G = 160 * V_G + 200$. Meanwhile Scaling the voltage from a range 0 to 5 V to yield the temperature in Kelvin in range 298 to 338 k done by $T = 8 * V_T + 298$.

$$I_{Ph} = (160 * V_G + 200)3{,}8m + [(8 * V_T)2{,}4m]$$
$$I_{Ph} = (160 * V_G + 200)3{,}8m + [(0{,}0192 * V_T)] \quad (9)$$

Equation 9 was used in Proteus and depicted in Figure 4 to yield the light generated current.

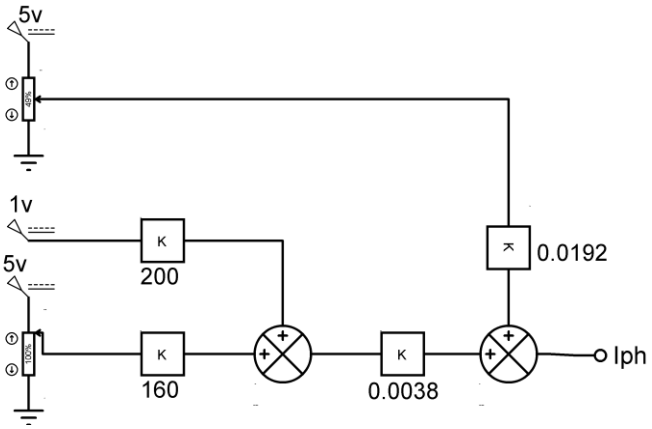

Figure 4. Modelling the light generated current.

Solving equations 2 and 3 yield:

$$I_s = \frac{I_{SC(STC)}}{\frac{q*V_{OC(STC)}}{e^{K_B*T_{STC}*N_s*n}} - 1}\left(\frac{T}{T_{STC}}\right)^3 * e^{\frac{-qE_g\left(\frac{1}{T}-\frac{1}{T_{STC}}\right)}{n*K_B}}$$

$$I_s = \frac{3{,}808}{\frac{1{,}602*10^{-19}*21{,}1}{e^{1{,}38*10^{-23}*298*36*1{,}045}} - 1}\left(\frac{T}{298}\right)^3 * e^{\frac{-1{,}602*10^{-19}*1{,}11*\left(\frac{1}{T}-\frac{1}{298}\right)}{1{,}045*1{,}38*10^{-23}}}$$

$$I_s = 1{,}245198 * 10^{-9}\left(\frac{T}{298}\right)^3 * e^{-12326{,}31606*\left(\frac{1}{T}-0{,}003355\right)} \quad (10)$$

Equation 10 was depicted in Proteus as shown in Figure 5 to yield the saturation or leakage current of the diode.

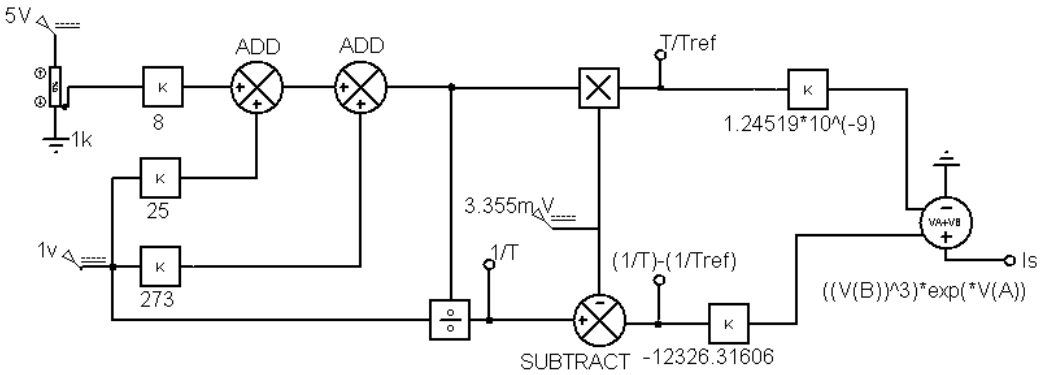

Figure 5. Modeling the saturation current of the diode.

$$I_D = \left(e^{\frac{1{,}602*10^{-19}(V+I_{PV}*0{,}316)}{1{,}38*10^{-23}*T*36*1{,}045}} - 1\right) * I_s$$

$$I_D = \left(e^{\frac{308{,}4663679(V+I_{PV}*0{,}316)}{T}} - 1\right) * I_s \quad (11)$$

Then, to determine the diode current, equations 11 and 6 were used in Proteus, as illustrated in Figure 6.

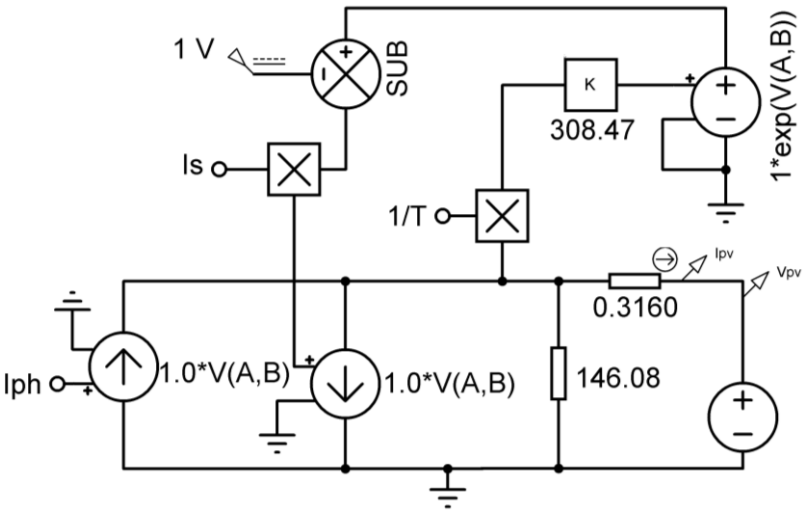

Figure 6. Modelling the diode current.

In Figure 7 the full MSX-60 model with the possibility of modifying both of the temperature varying from 25℃ to 65℃ and irradiation changing from 200 up to 1000 $\frac{\mathrm{W}}{\mathrm{m}^2}$ has been done in Proteus software. As the MSX_60 has been modeled, the second step is to test the validity of our proposed system, as depicted in Figure 7. From the first glance, comparing the IV and PV of our modeling under different operating conditions with the data given in the datasheet look like the best choice. Here in this work, the IV and PV solar characteristics of $1000\frac{\mathrm{w}}{\mathrm{m}^2}$ and $200\frac{\mathrm{w}}{\mathrm{m}^2}$irradiations with different temperature setpoints 25 ℃, and 65 ℃ are shown in Figure 8. The temperature has negative effect on both of voltage and power, meanwhile irradiation has positive effect due to increase in the number of photons hitting the surface.

With the increase of light intensity, the maximum output power, short-circuit current, and open-circuit of the solar cells increase. Therefore, the higher the light intensity, the higher the output current and generated power will be.

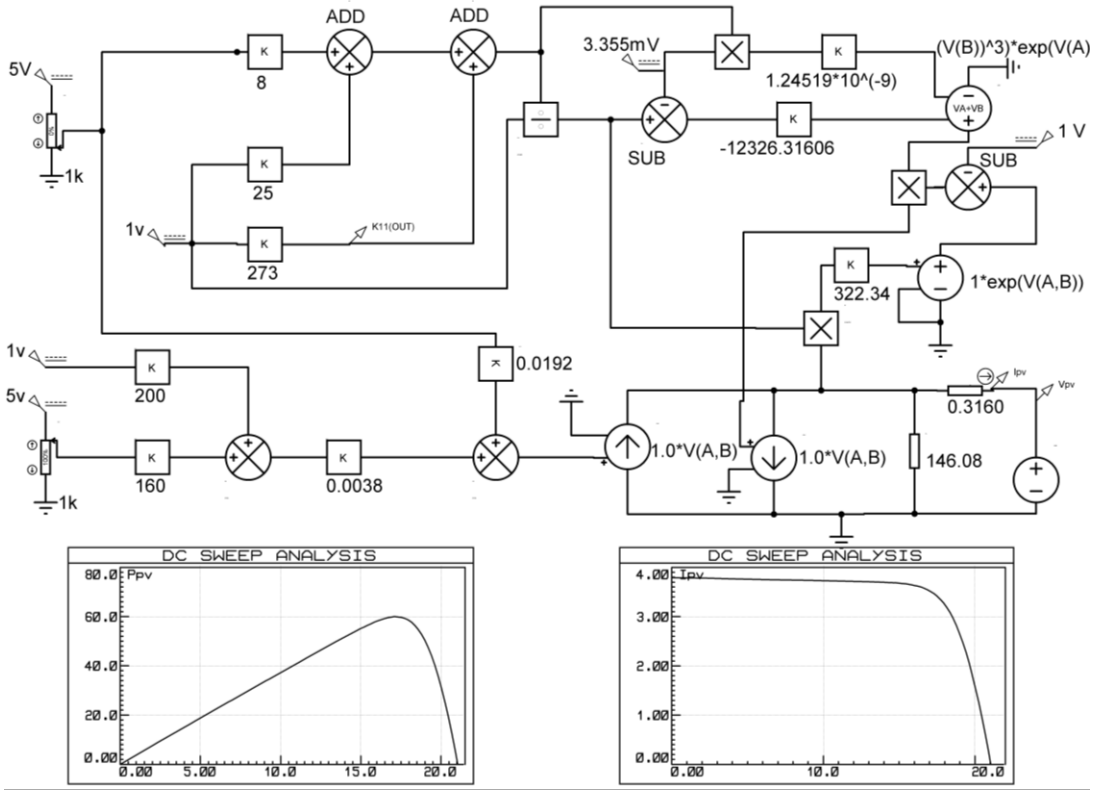

Figure 7. Modelling MSX-60 PV panel.

It is an irrefutable fact that bandgap mitigation is associated with increasing the temperature, in consequence, the more electron-hole pairs are created, and an increase in the energy of elections can be clearly seen. In this context, a slight increase in the short circuit current from 3.792 A to 3.888 A was occurred with increasing the temperature from 25℃ to 65℃ under 1000 $\frac{W}{m^2}$ irradiance. On the other hand, the behavior of reverse saturation current is proportional with the square of the intrinsic carrier concentration, which in term has an exponentially inverse relation with the band gap energy. As a result of that impact, decreasing the fill factor value and the open circuit voltage are expected with increasing the temperature. In Figure 8, the open circuit voltage dropped from 21.05 V to 18.1 V with increasing of the temperature with 40 ℃ above the room temperature. As a result, the temperature coefficient behavior of the short-circuit current and the open-circuit voltage is reversed. In that regard, increasing the temperature leads to decrease in the maximum power, because the decrease in the maximum voltage does not compensate the increase in the maximum current.

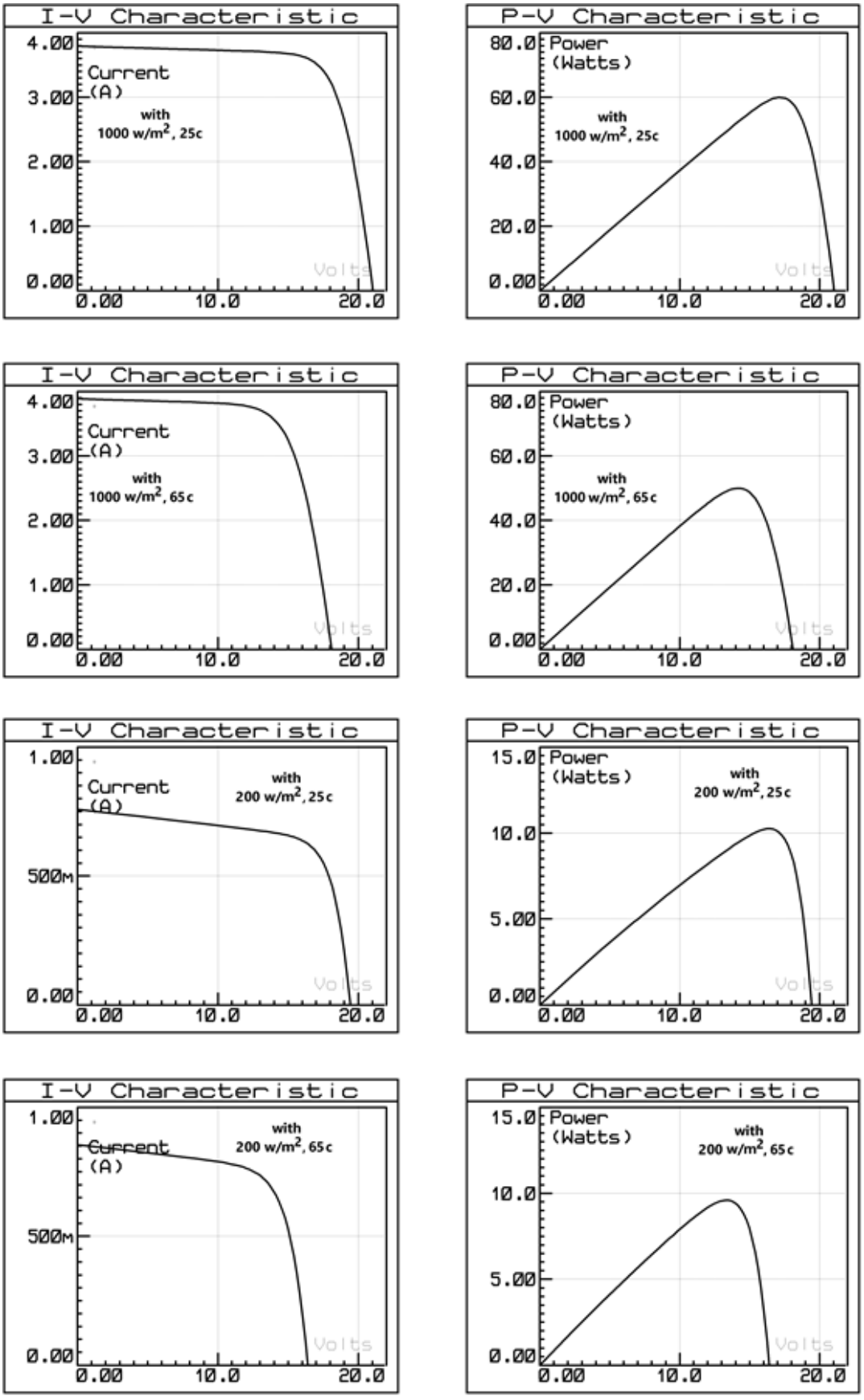

Figure 8. I-V and P-V characteristics of our model for MSX-60 panel and different temperature and irradiation values.

2.2. Keypad

Besides selecting the primary desirable output voltage of the system, the other crucial feature developed by the authors associated with keypad work is the flexibility to adjust the output voltage at any time by pressing on # to increase it by one, or * to decrease it by one, with putting in our consideration the maximum and minimum allowable adjustment which is done by software.

2.3. Buck converter analysis

In Figure 9, the duty cycle of the MOSFET represents the control variable, with $\frac{1}{T_s}$ switching frequency. The MOSFET is 'off' during the interval $(1-d)T_s$ and 'on'during dT_s.

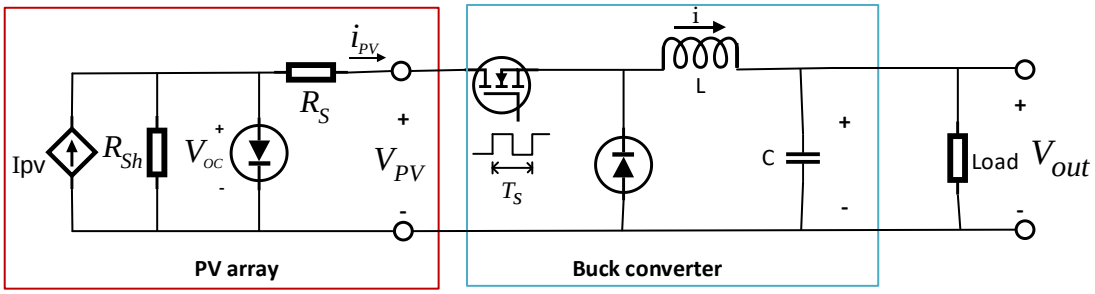

Figure 9. Schematic diagram for step down converter fed by PV array.

The principle behind the buck converter mechanism is to supply a voltage with a range from zero up to the input value. Its operating principle is manipulating the duration of time in which the energy is granted to the inductor. Two modes are sub-divided under the Continuous Mode Power Supply (CMPS). For the circuit in Figure 10a, mode1 starts at t=0 when the switch is turning on. In this case, the source input supplies energy directly to the inductor, and the diode is reversely biased. The second mode is shown in Figure 10b. In which both the inductor and capacitor contribute to supply the energy to the load.

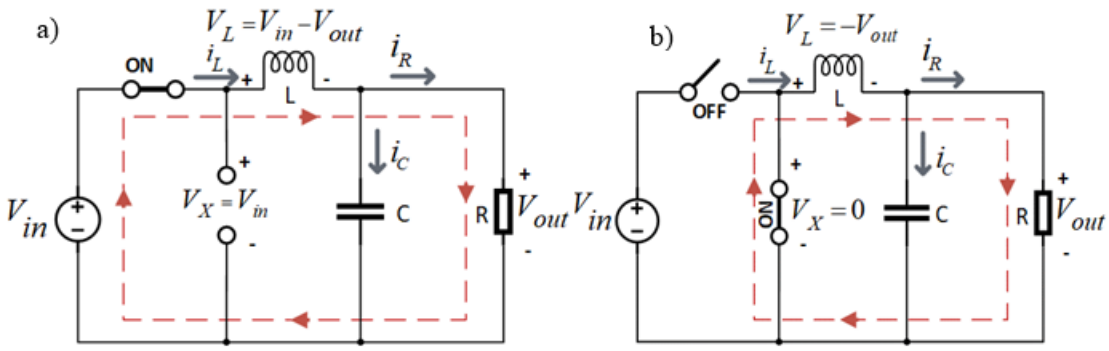

Figure 10. a) Switching ON mode for the buck converter. b) Switching OFF mode

In general, the input voltage is greater than the output voltage and is expressed as (Rashid, 2011).

$$V_{in} = \frac{V_{out}}{D} \quad (12)$$

where V_{in} is the input voltage from MSX-60 solar panel, and V_{out} is input voltage, and D is duty cycle. To avoid falls the converter behind the discontinuous mode case, there must be no period of a zero-inductor current between switching off and on period, the critical inductor value expressed as (Rashid, 2011):

$$L_{Critical} = \frac{(1-D)R}{2f} \quad (13)$$

The minimum inductance value is $L_{Critical}$, f is the switching frequency, which is 30k Hz, and R is the output resistance, which is 7Ω.

To overcome the DMPS, the minimum value of inductance had calculated with the following constraints: input voltage 21 V and desirable output voltage 8 V.

$$L_{Critical} = \frac{\left(1-\frac{8}{21}\right)*7}{2*30k} = 7{,}222*10^{-5}\,H$$

For safety L> 1,4 $L_{Critical}$

$$L = 1{,}3*10^{-4}\,H = 130\mu H \quad (14)$$

For matching the desired ripple of the output voltage, which is 0,03, the minimum capacitor value is (Rashid, 2011).

$$C_{min} = \frac{(1-D)V_{out}}{8Lf^2\Delta V_{out}} \quad (15)$$

$$C_{min} = \frac{\left(1-\frac{8}{21}\right)*8}{8*1{,}3*10^{-4}\,(30k)^2*0{,}03} = 176{,}3\ \mu F$$

The capacitor value has been taken as, C=200µF.

$$C{=}200\mu F \quad (16)$$

2.4. Proportional Integral Implementation

PI controller is very well known by engineers and researchers working in related fields. However, when the PI algorithm is implemented with microcontroller applications, the situation becomes a bit complicated and requires knowledge not easily available in the technical literature.

The aim behind this section is to overcome the lack of technical information about employing PI controller in the discrete domain after converting it from the conventional analog from, which associated with the microcontroller usage.

This detailed analysis and the derivation of the PI controller in discrete domain with a microcontroller and using it to get access to constant output voltage under different external ambient conditions will provide important contributions to researchers.

According to the literature, the factor K_i multiplied by the area under the curve represents the integral part, from Figure 11 the bounded area between (aT-T) and (aT) can be pictured as a trapezoid.

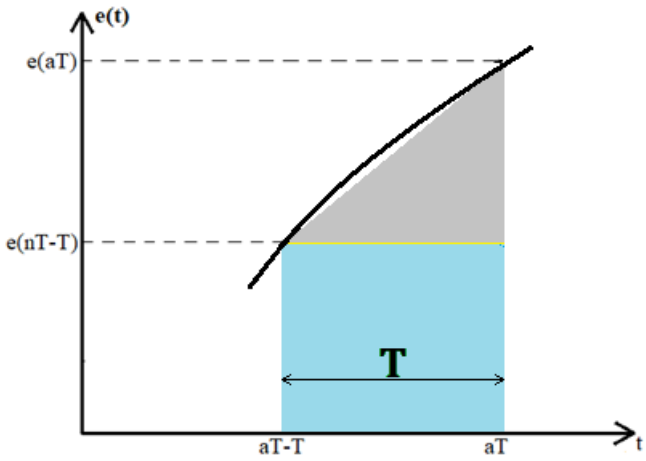

Figure 11. Demonstration of the PI controller integral part.

$$y_{(t)} = K_i \int_0^t e_{(t)}.dt = \left(K_i \int_0^{aT-T} e_{(t)}.dt\right) + \left(K_i \int_{aT-T}^{aT} e_{(t)}.dt\right) \quad (17)$$

For the below equation, the area up to $(aT - T)$ is represented by $y_{(aT-T)}$, and the incremental area for T period are represented by $\Delta y_{(aT,aT-T)}$.

$$y_{(aT)} = y_{(aT-T)} + \Delta y_{(aT,aT-T)} \quad (18)$$

By investigating Figure 11 the trapezoid area can be taking apart into two parts triangle and rectangle as it explains in the below equation.

$$\Delta y_{(aT,aT-T)} = K_i \left(\frac{1}{2} * T\left(e_{(aT)} - e_{(aT-T)}\right) + T * e_{(aT-T)}\right) \quad (19)$$

$$\Delta y_{(aT,aT-T)} = \frac{TK_i}{2}\left(e_{(aT)} + e_{(aT-T)}\right) \quad (20)$$

By substituting equation 18 in 20 yielded to

$$y_{(aT)} = y_{(aT-T)} + \frac{TK_i}{2}\left(e_{(aT)} - e_{(aT-T)}\right) \quad (21)$$

Taking the Z-transform yielded in

$$Y_{(z)} = Y_{(z)}Z^{-1} + \frac{TK_i}{2}\left(E_{(z)} + E_{(z)}Z^{-1}\right) \quad (22)$$

So, the transfer function of the integral part is

$$\frac{Y_{(z)}}{E_{(z)}} = \frac{TK_i}{2}\left(\frac{Z^{-1}+1}{Z^{-1}-1}\right) = K_i\frac{T}{2}\left(\frac{1+Z}{Z-1}\right) \quad (23)$$

With combining the integral and proportional parts

$$\frac{Y_{(z)}}{E_{(z)}} = K_p + K_i\frac{T}{2}\left(\frac{1+Z}{Z-1}\right) \quad (24)$$

$$\frac{Y_{(z)}}{E_{(z)}} = \frac{K_p(Z-1)+\left(K_i\frac{T}{2}*(1+Z)\right)}{Z-1} = \frac{\left(Z*(K_p+K_i\frac{T}{2})\right)+(-K_p+K_i\frac{T}{2})}{Z-1} \quad (25)$$

$$\frac{Y_{(z)}}{E_{(z)}} = \frac{(K_p+K_i\frac{T}{2})+\left(\left(-K_p+K_i\frac{T}{2}\right)*Z^{-1}\right)}{1-Z^{-1}} \quad (26)$$

$$Y_{(z)} - Z^{-1}Y_{(z)} = (K_p + K_i\frac{T}{2})E_{(z)} + (-K_p + K_i\frac{T}{2})Z^{-1}E_{(z)} \quad (27)$$

$$y_{(n)} = y_{(n-1)} + \left(K_p + K_i\frac{T}{2}\right)e_{(n)} + \left(-K_p + K_i\frac{T}{2}\right)e_{(n-1)} \quad (28)$$

Equation 28 is used as the base for implementing the Proportional-Integral algorithm via the microcontroller. PI parameter has found by the trial and error as the following $K_{p=}0{,}5589359$ and $K_i = 21{,}41635$.

2.5. Mapping

In Figure 2, two mapping processes have been represented. First one executed by software on microcontroller which is responsible for changing the range of the PI controller output to another range represent the duty cycle. The second mapping process executed hardware for feeding back the output voltage by using voltage divider to protect the microcontroller from overvoltage.

2.5.1. Software mapping

Software mapping is used to adjust the PI controller output range to another scale representing the duty cycle, the details and deriving are explained below.

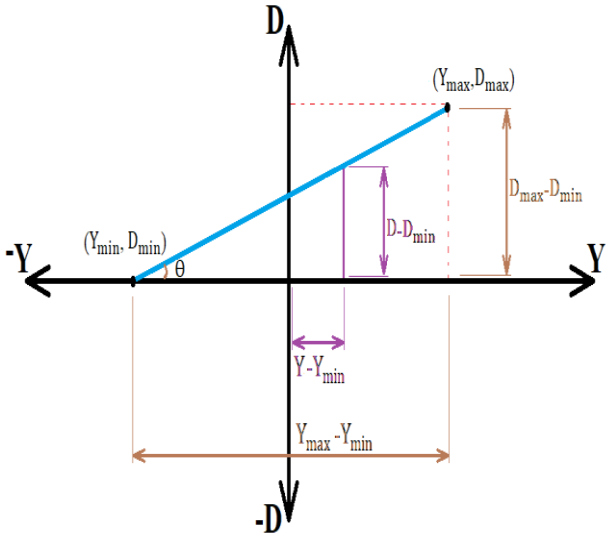

Figure 12. Mapping between PI output value and duty cycle.

By looking closely to Figure 12 and from similar triangular method we can infer:

$$\tan\theta=\frac{Y_{max}-Y_{min}}{D_{max}-D_{min}}=\frac{Y-Y_{min}}{D-D_{min}} \tag{29}$$

Where Y represents the output of PI controller, meanwhile D represents the duty cycle

$$D-D_{min}=(Y-Y_{min})\left(\frac{D_{max}-D_{min}}{Y_{max}-Y_{min}}\right)$$

$$D=\left((Y-Y_{min})\left(\frac{D_{max}-D_{min}}{Y_{max}-Y_{min}}\right)\right)+D_{min} \tag{30}$$

Equation 30 was used as the base for swapping the PI controller output to a duty cycle.

2.5.2. Hardware mapping

The proposed circuit design depicted in Figure 13 supplies maximum output voltage reaching up to 21,1 V, due to constrains associated with the microcontroller, the maximum allowable voltage that could be sensed by PIC18F4580 without damaging it is 5 V, so in this case using voltage divider is a must. The process of scaling the sensible voltage was done on microcontroller by multiplying it with 4,22 to convert it from 0-5 V safe input range up to 0-21,1 V.

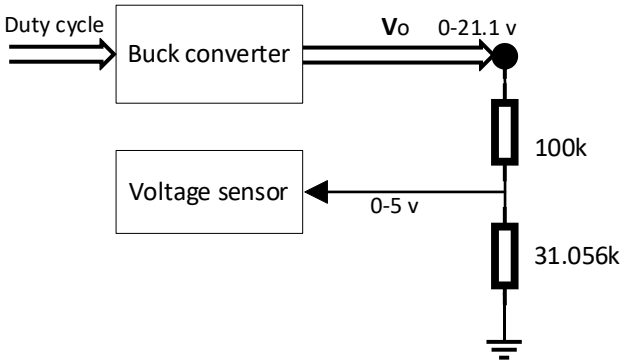

Figure 13. Hardware mapping for feeding back the output voltage.

2.6. Final Circuit Implementation and the Code Algorithm

While working with solar cells, it is crucial to grasp the effect of temperature and irradiation on efficiency. With this regard, the negative impact of increasing the ambient temperature and the positive influence of increasing the irradiation throughout the day is depicted in Figure 8. For specific simple applications, like installing a panel on the rooftop of a pavilion for running an alarm system or simple communication purposes or even charging mobile batteries, supplying steady voltage throughout the day under different ambient circumstances is a must. This work proposes to fill the lack of information about implementing tracking techniques in MCU. The system was designed and tested in Proteus 8. The main blocks and components in this work are:

2.6.1. PIC18F4580 Microcontroller and the keypad

In this section, PIC18F4580 was used. The MCU pins and keypad configurations were connected as depicted in Figure 14.

- Port B was used to connect between the MCU and the keypad.
- LCD connected pins C_0, C_1, C_3, C_4, C_5, E_0.
- MCLR - Master Clear Pin External Reset was connected with a circuit as recommended in PIC18F4580 datasheet (Microchip, 2007).
- A_2 pin: the output voltage of the buck converter was sensed and entered pin A_2.
- A_3 pin: the output value of the solar cell module was entered with the possibility to sense and display it on LCD even when the temperature and irradiation were changed.

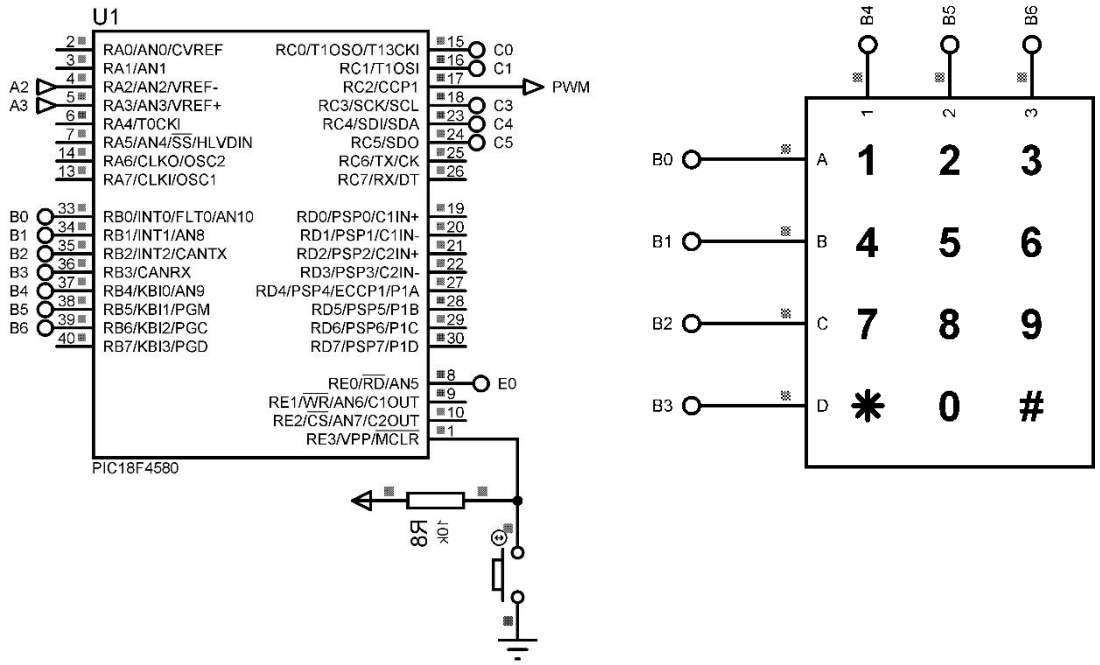

Figure 14. Keypad and PIC18F4580 implementing part.

2.6.2. LCD, Oscilloscope and MSX-60 PV panel

To keep the user in touch with the system, a 16*2 LCD was used. When the simulation is initiated; a welcoming message appears on LCD to ask the user to enter the desirable voltage. If it is with the accepted range, higher than 4 V and less than 15 V, the desired voltage, actual voltage, duty cycle, and the output voltage of the PV module appear in the LCD columns.

With the oscilloscope:

- The output voltage of the buck converter versus time is displayed
- Duty cycle of the system and the way of changing it concerning the desired voltage, which is inferred from dividing the output voltage from the buck converter on the output voltage from the PV module are presented
- Irradiation and temperature are displayed

Figure 15 shows the LCD, oscilloscope, and the subcircuit of MSX-60 PV panel with the existence of DC link capacitor with 25 μF. The function of the capacitor is energy storage as potential energy. So, it can supply the load when the source is reduced and it will store the surplus power in case of Generator excess, serving as regulator and stabilizer between the source and the load. As it increases, it will store more energy and can fix the voltage for longer time.

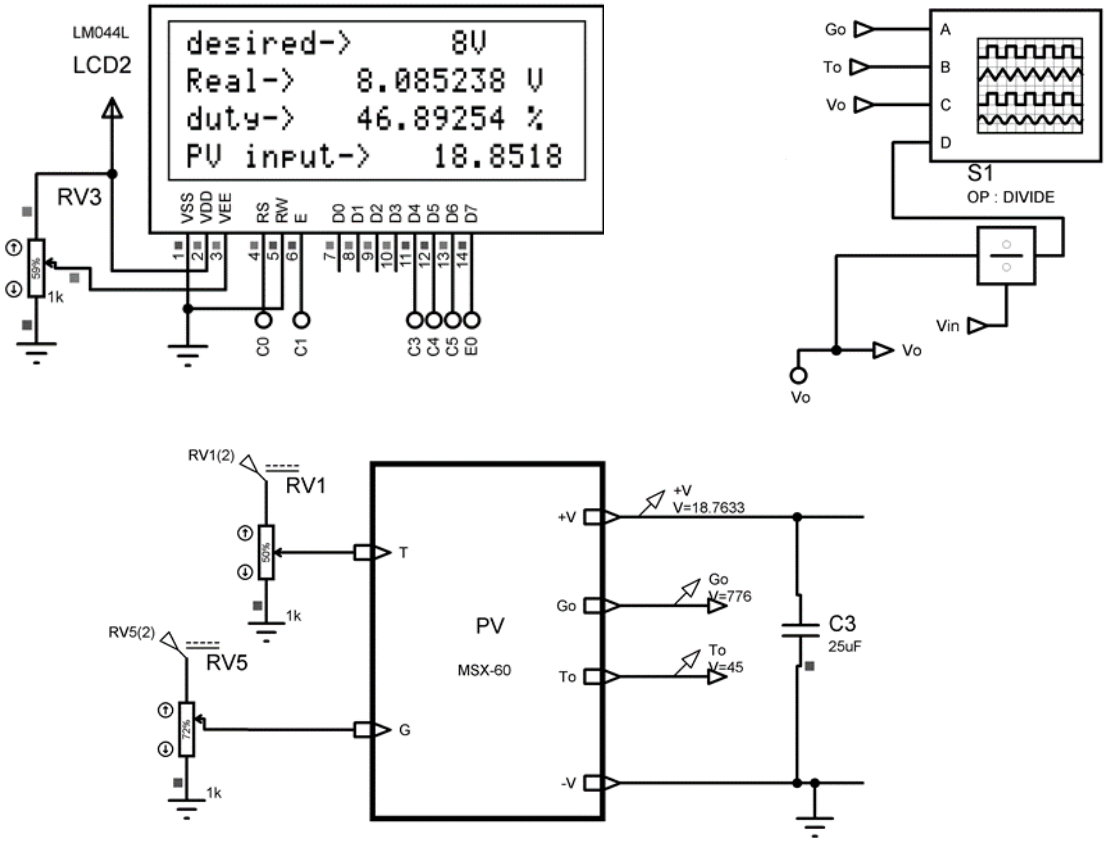

Figure 15. LCD, Oscilloscope and MSX-60 PV panel.

2.6.3. Bootstrap circuit and Buck converter

The proposed schematic represented in Figure **16** includes stepdown converter and its bootstrap with the following buck converter parameters: switching frequency 30 kHz, an inductor (L=130 μH), duty cycle ratio (0-100), and capacitor (C=200 μF) have determined based on equations 14 and 16. IR2112 has been used as a bootstrap to pull up the operating point of the N-type MOSFET above the solar cell rail for enabling to push the transistor to operate during the ON mode.

F represents the whole system formed after combining Figure 14, Figure 15 and Figure **16**. The proposed system has been tested with 8 V desirable input voltage from the keypad; the MCU did the necessary task to present it on the LCD and implementing the discrete PI algorithm on the system. Before importing the PWM signal into N-channel MOSFET and energize the switch to run in the ON period, it is crucial to ensure the PWM amplitude is higher than the thresholding voltage. According to PIC18F4580 specifications, the output PWM voltage ranging from 0 to 5 V, IR2112 circuit is responsible for scaling this signal to a higher range. In the end, the output voltage and the duty cycle has presented in the other columns of the LCD.

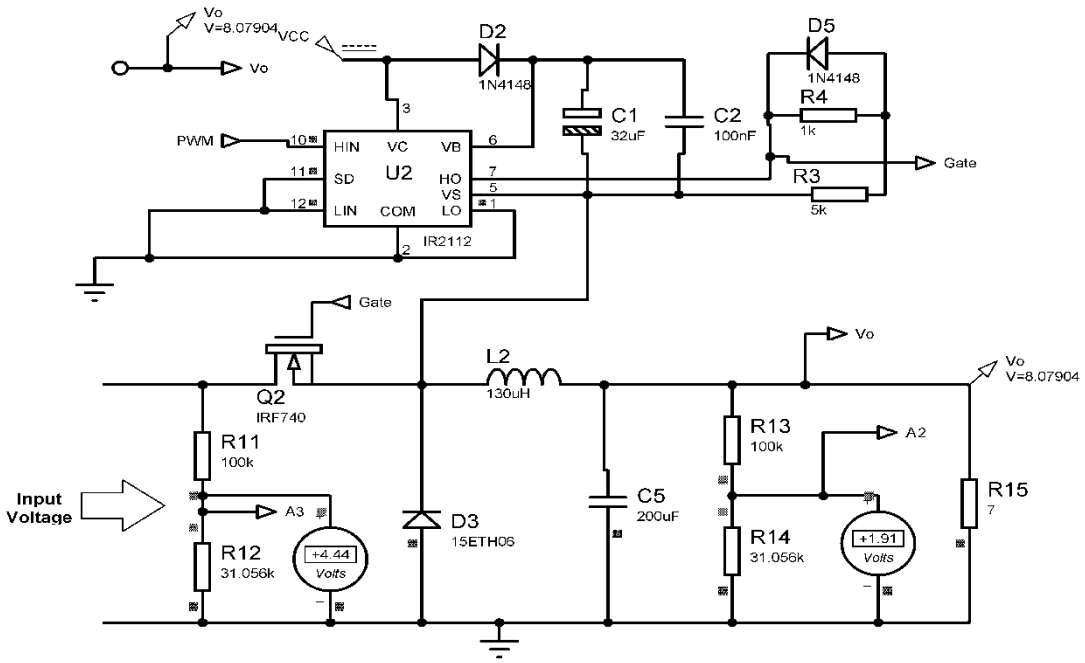

Figure 16. Bootstrap circuit and Buck converter.

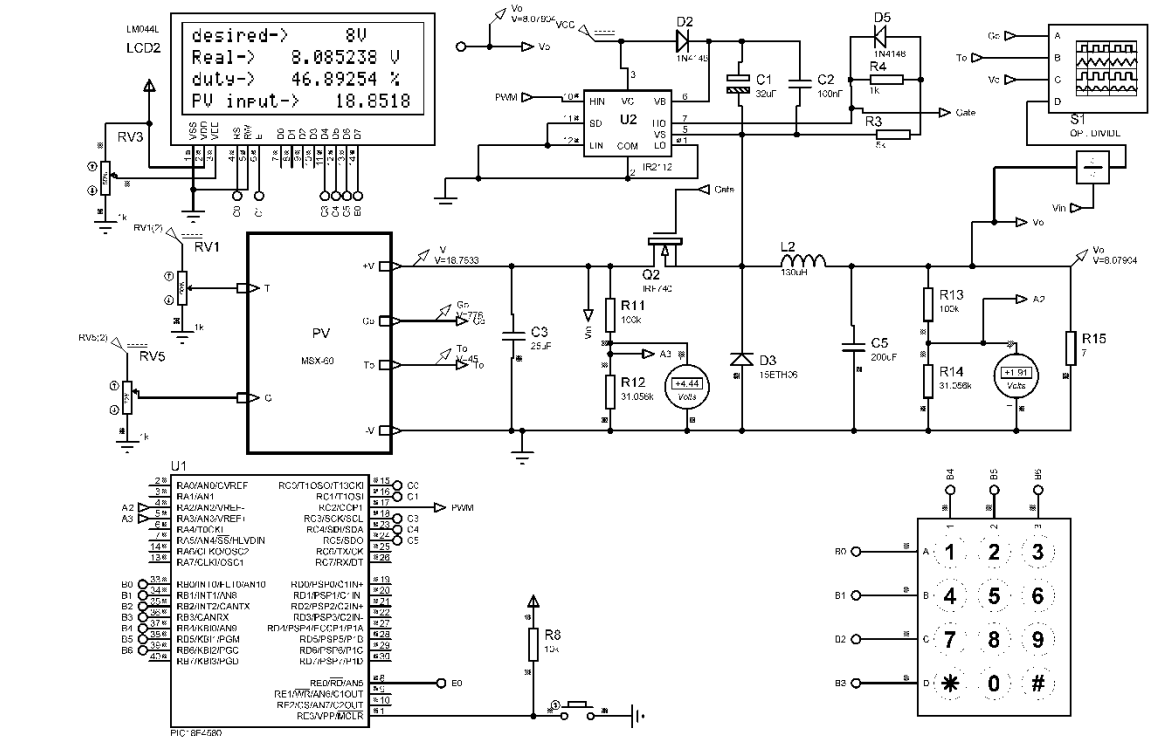

Figure 17. The system schematic diagram of Buck converter fed by PV panel.

Describing the details of the algorithm is one of the main goals behind this work, as presented in Figure 17. Since it contains a lot of information, it is divided into subgroups for simplifying purposes. In this context, they are as described below:

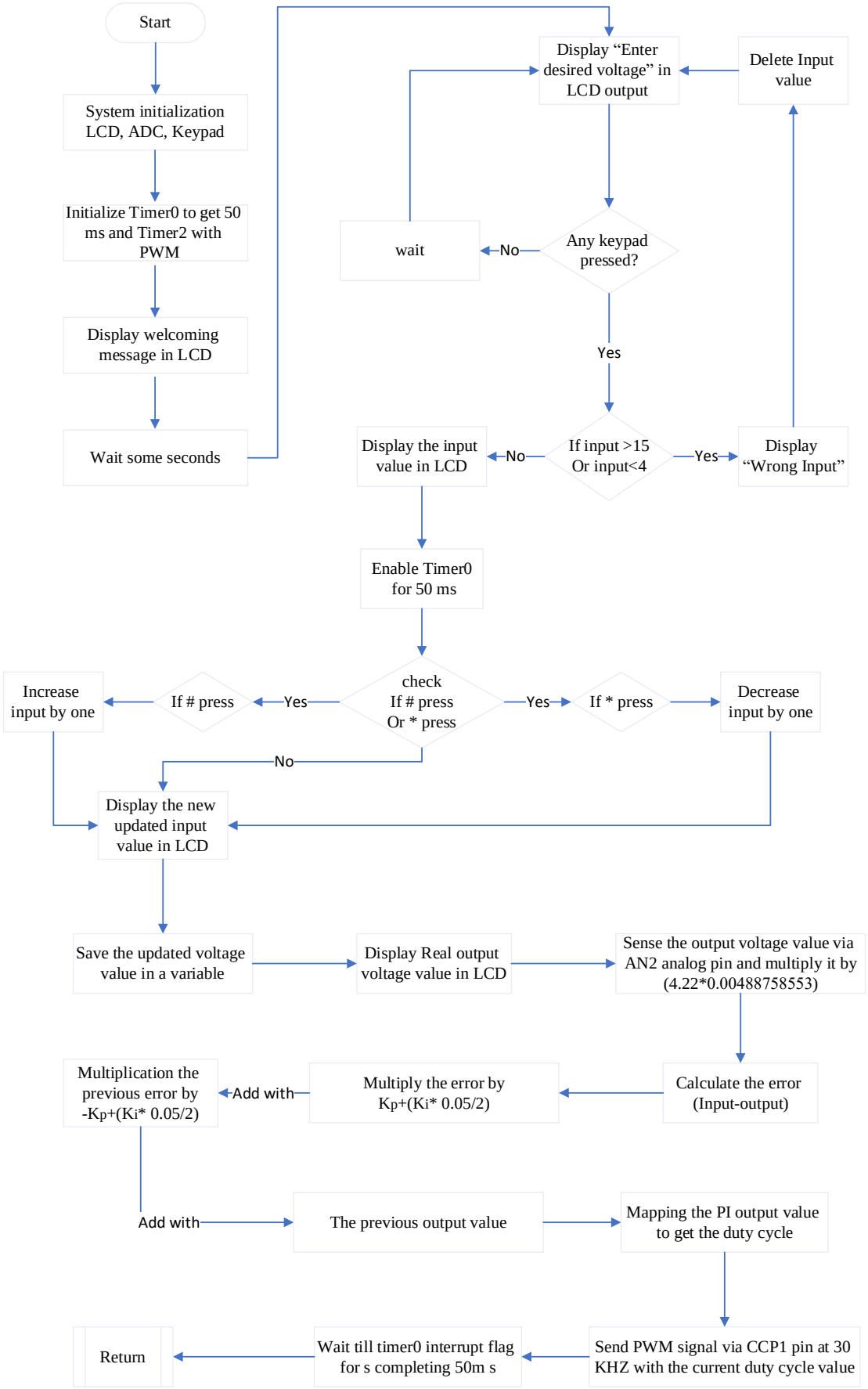

Figure 17. Flowchart for the proposed algorithm.

- The initialization and configuration of Keypad, LCD, ADC, Timer0, and Timer2. In our case with PIC18F4580, the system has been designed and initialized in this way; if the input voltage is not with the range of 5 to 15 V, the user sees a warning message on the LCD saying it was a wrong input. Furthermore, this part includes the initialization of Timer0 for timing 50 ms, Timer2 to control the PWM signal, ADC registers to control sensing the actual voltage as need. T0CON= 0x00; TMR0H = 0x50; TMR0L= 0x38; crystal frequency 8 MHz, Channel 1, 2 to deal with the ADC.
- After the preliminary selection of the desired input, the system enables 50 ms by Timer0 as a sample time to match the pre-requirements of implementing time-varying discrete algorithms. In this part, the system is flexible to modify the desired voltage at any time with the keypad. In the end, the desired value should be saved in a variable whether it has been updated or not.
- Presenting the desired input voltage on LCD is the first thing done in this part. The output voltage of the PV cell or the PV cell module under different temperatures or irradiations is sensed accurately by taking into account to prevent any possible damage to the microcontroller caused by the excessive voltage. In this context, a voltage divider circuit has been used to scale the 0 to 21,1 V to a range of 0 to 5 V. On the other hand, the MCU rescale values these back by multiplying with 4,22.

  At the end of this part, the actual buck converter voltage could be sensed via the help of AN2 ADC input pin and multiplied by (4,22*0,00488758553). The previous value 0,00488758553 was deducing from dividing 5 V on 1023, where 1023 is the number of levels in ADC, which comes from the fact that PIC18F4580 contains 10 bits. This way guarantees to protect the MCU from burning without effect on the accuracy of measurements.
- In this part, it is shown that subtracting the actual voltage from the desired one forming the error. The error value is saved as a current variable value to multiply by 0,612476 according to equation 28.

  Multiply the error by $K_p + \left(K_i * \frac{T_s}{2}\right)$

  K_p is 0,5589359, K_i is 21,41635, and T_s is 50 ms.

  This outcome adds with the multiplication of the previous error value by $-K_p + \left(K_i * \frac{T_s}{2}\right)$

$$\text{drive}=\left(K_p + \left(K_i * \frac{T_s}{2}\right) * \text{current error value}\right)+\left(-K_p + \left(K_i * \frac{T_s}{2}\right) * \text{privoust error value}\right)$$

  The value of the above equation added to the previous value of the final PI outcome of equation 28. To import the PWM signal in circuit switch with suitable duty cycle value, mapping it from the current range to a range from 0 to 255 because the controlling register of PWM signal is Timer2 which consists of 8 bits.

3. Circuit Simulation Results and Discussion

The validity of the designed system has been tested under different weather conditions to bring it closer to reality.

In order to be aware of the proposed research's status concerning the stand-alone case without a battery system, a brief literature review was considered by the authors. At the beginning of the study, due to the absence of the PV device in Proteus, which is one of the most common platforms used with MCU, a lot of uncertainty came with (Ghani et al., 2019) results when DC voltage source was used instead of the PV device. In the studies of researchers who saw this deficiency, such (Salman et al., 2018), skip the simulation part on Proteus and went through implementing the hardware circuit directly without the pre-checking with trusted platforms for the same aforementioned reason.

Furthermore, the difficulties associated with utilizing the MCU unit in the Discrete PI controller are rarely found elsewhere, because most researchers didn't prefer the challenging route and they implemented it with Arduino (Suroso et al., 2020) which would restrain with specific libraries and specific pre-set algorithms. In this context, others concentrated on implementing their system on MATLAB, if it was hardware or just simulation on MATLAB, without the capability to implement on Proteus (Doubabi et al., 2018; Ergin Şahin, 2020).

Although (Geethanjali and Sidram, 2018; Motahhir et al., 2018; Chalh et al., 2020) works, can be considered as the closest to proposed work, there is a big difference. They have simulated the PV system with Proteus but without the ability of modifying the weather conditions, and they tracked the MPPT without any consideration of tracking the desired voltage with the discrete domain, which is considered as the most challenging part in this field. With the success of validating our proposed system, based on our PI discrete domain derivation, future work including another traditional control algorithm is planned to be implemented in the discrete domain. The results of whole system will be re-validated by implementing the system with the hardware part.

As mentioned in the buck converter section, the directly proportional relationship between the actual voltage and the duty cycle has been confirmed successfully as shown in Figure 18. In which the desired voltage can be modified while the simulation is running.

At the beginning the user opted for 10 V as the desired input voltage with irradiation and temperature values of 520 $\frac{W}{m^2}$ and 65 ℃ respectively, the implemented PI algorithm in the discrete domain showed itself by increasing the duty cycle to a value in which the output voltage matches the desired one around 0,61. After the voltage settled down, a modification in the desired voltage value occurred; via pressing two times on* from the keypad to be 8 V. Again, the PI algorithm played a pivotal role in decreasing the duty cycle to 0,485 to match our requirements. In the end, the duty cycle reaches to 0,358 value when the desired voltage is 6 V. With all of these aforementioned results, the direct relationship between the actual voltage and the duty cycle has been proven successfully.

The validity of our algorithm to make a perfect voltage tracking regardless of the ambient temperature has been proved as depicted in Figure 19. In this case: the system parameters have been chosen as 8 V desired voltage and 520 $\frac{W}{m^2}$ irradiation, while the temperature is changeable via the help of the potentiometer and its mapping accessories circuit. As the simulation started running at 65 ℃ ambient temperature, the supplied voltage from the MXS-60 panel to the buck converter was 16,65 V. The system showed a good response regarding tracking the 8 V desired voltage. Decreasing the temperature down to 50 ℃, the MXS-60 supplied voltage immediately reacted to that change and became 17,85 V, according to the reverse relationship between them. 40 V

When the temperature is decreased to 25 ℃, the panel supplied voltage reached to 19,9 V. At the temperature decrease point, the actual voltage went up with a huge jump compared to other fluctuations. Because the system previously was stabilized with a specific duty cycle, then as the input voltage went up, due to decreasing the temperature, the high duty cycle of the previous step with this updated input voltage value led to that unusual jump. As time goes on, the PI algorithm shows itself and restrain the duty cycle to new smaller one.

Depicted the case of exposing the system to varying irradiation under 65 ℃ and 8 V desired voltage. The process has started with 320 $\frac{W}{m^2}$ incident irradiation, and the input voltage reached up to 15,85 V. The direct proportional relationship has appeared clearly as the irradiation reached to 520 $\frac{W}{m^2}$ pushing the MSX-60 supply voltage to be 16,8 V. An excellent voltage tracking has been shown to disturb the system by manipulating the irradiation up to 1000 $\frac{W}{m^2}$ by decreeing the duty cycle value, and hence the system keeps tracking the desired voltage.

It is highly important to mention about the number of fluctuations in each square of the time axis, there are five mini- swings. These fluctuations per 250 ms explained as the sampling time was 50 ms, so for each unique 50 ms there must be an output duty cycle value transmitted from the PWM pin. In other words, there is an output voltage value each 50 ms. So, with a 250 ms time scale, it should contain the required number of fluctuations.

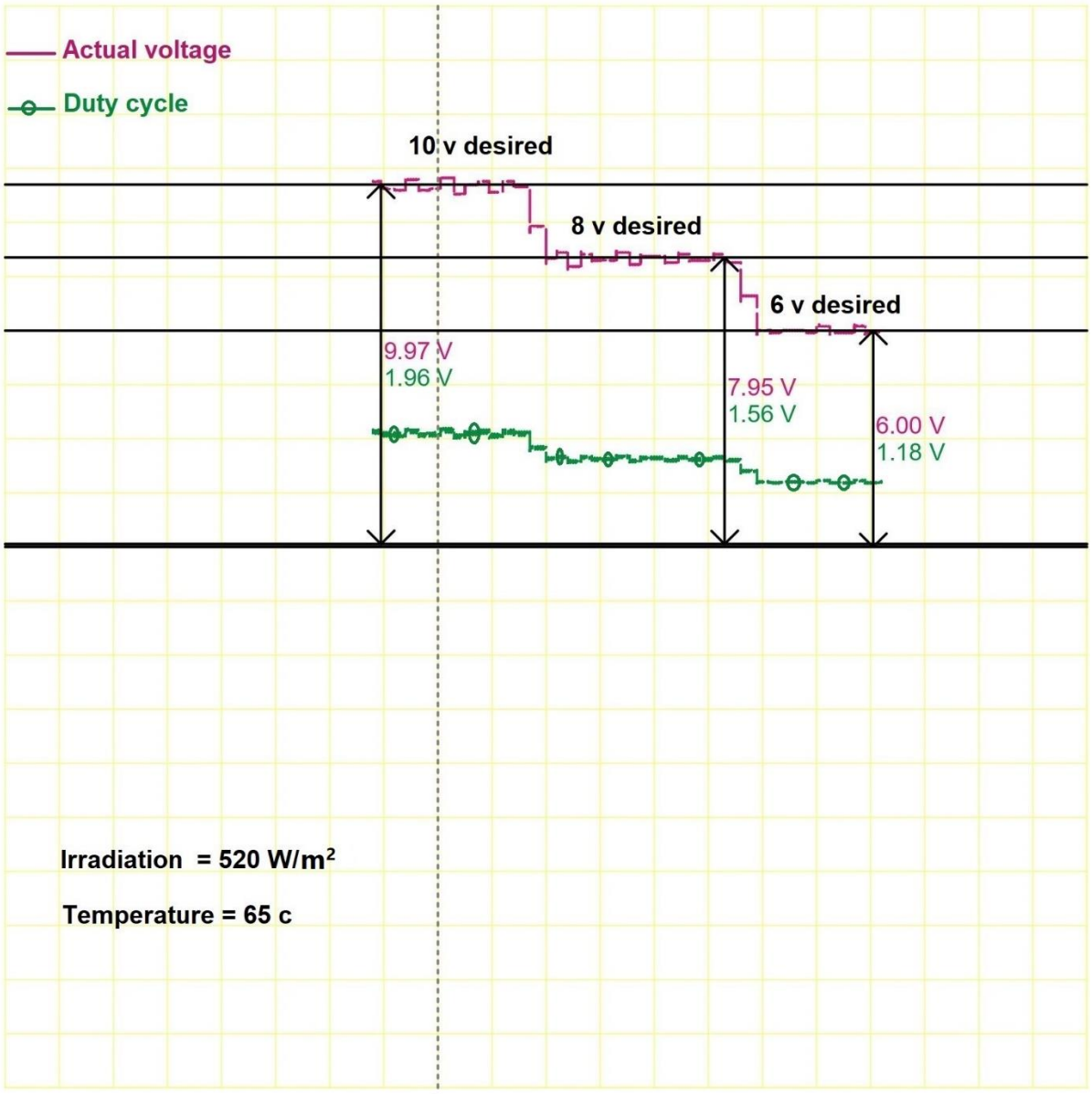

	Channel A	Channel B	Channel C	Channel D
V/Div	50.00 V	10.00 V	1.50 V	295.00 mV
Offset	-1000.00 V	0.00 V	0.00 V	0.00 V
Invert	Normal	Normal	Normal	Normal
Coupling	Off	Off	DC	DC

Horizontal		Trigger	
Source	Trace	Source	Channel A
Position	2.00 S	Level	-200.00 V
S/Div	250.00 mS	Coupling	DC
		Edge	Rising
		Mode	Auto

Figure 18. Effect of manipulating the desired voltage on the output voltage and the duty cycle, under 520 w/m^2 and T=65 °C.

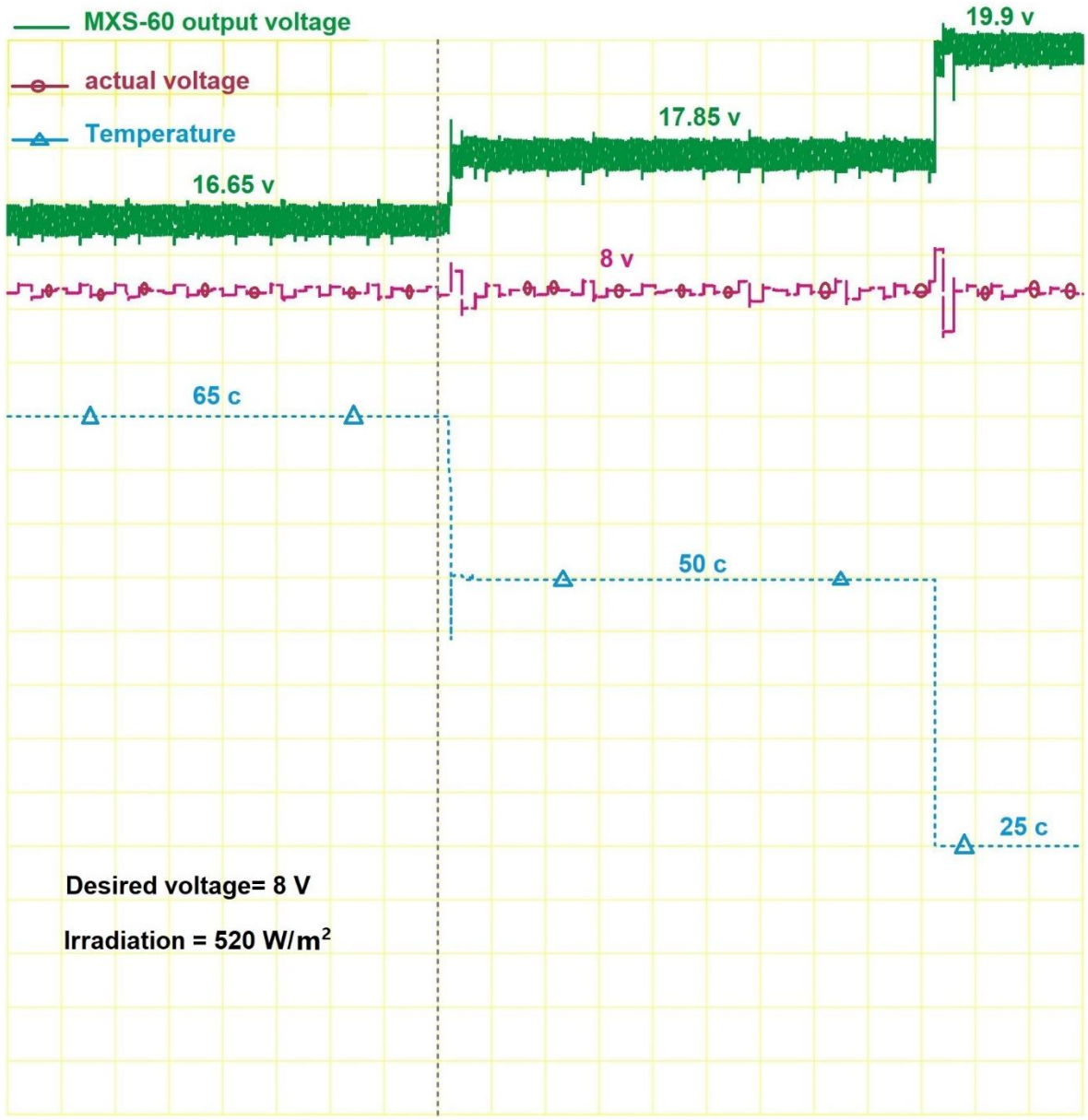

	Channel A	Channel B	Channel C	Channel D
V/Div	50.00 V	5.00 V	1.50 V	1.00 V
Offset	-1000.00 V	-100.00 V	0.00 V	-20.00 V
Invert	Normal	Normal	Normal	Normal
Coupling	Off	DC	DC	DC

Horizontal		Trigger	
Source	Trace	Source	Channel A
Position	2.00 S	Level	-200.00 V
S/Div	250.00 mS	Coupling	DC
		Edge	Rising
		Mode	Auto

Figure 19. Effect of changing the temperature on the PV voltage and the actual voltage under 520 W/m^2 and 8 V desire voltage.

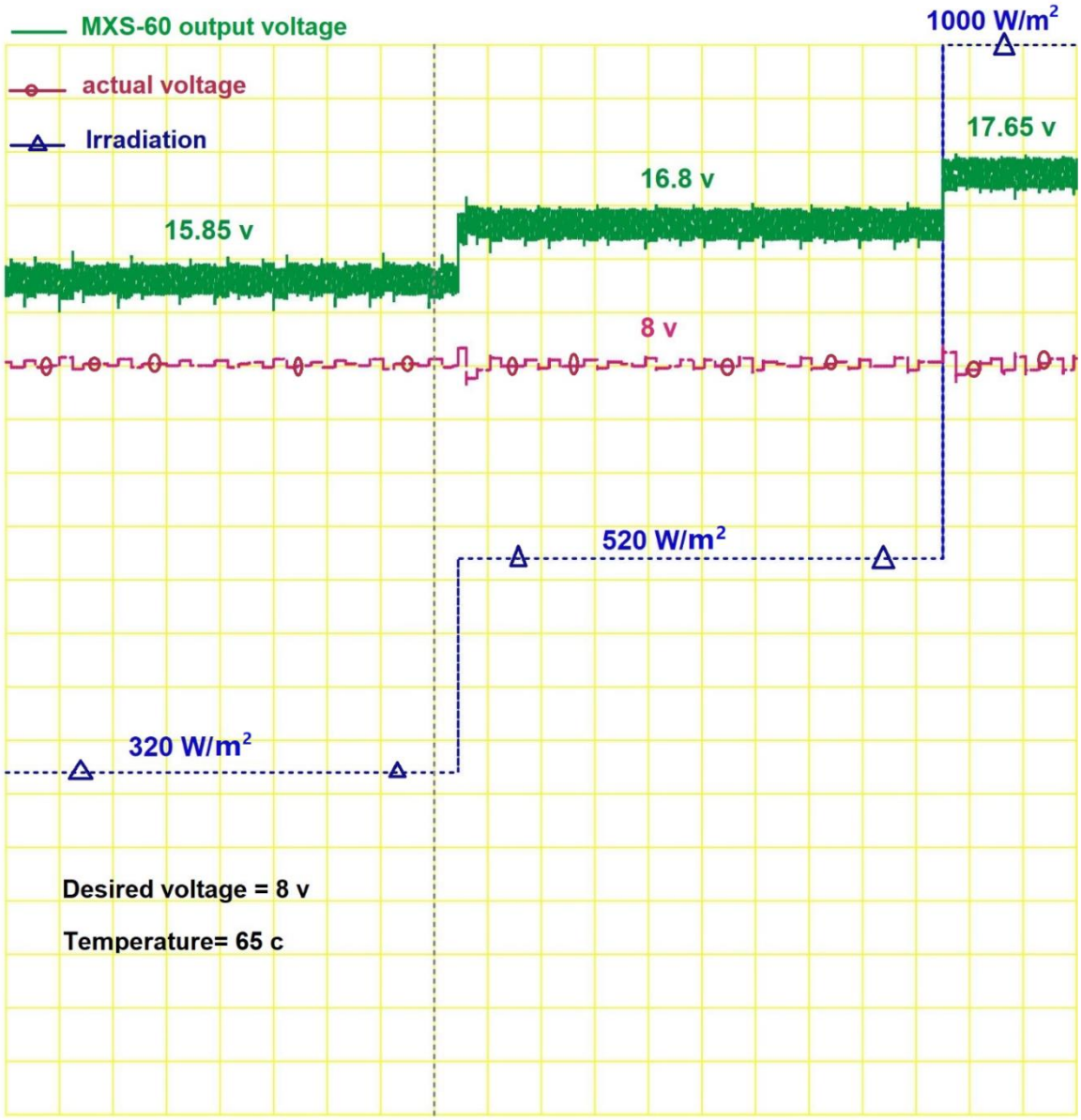

	Channel A	Channel B	Channel C	Channel D
V/Div	50.00 V	50.00 V	1.50 V	1.00 V
Offset	-1000.00 V	-1000.00 V	-3.90 V	-20.00 V
Invert	Normal	Normal	Normal	Normal
Coupling	Off	DC	DC	DC

	Horizontal
Source	Trace
Position	2.00 S
S/Div	250.00 mS

	Trigger
Source	Channel A
Level	-200.00 V
Coupling	DC
Edge	Rising
Mode	Auto

Figure 20. Effect of changing the irradiation on PV input voltage and the actual output voltage under 65 °C, and 8 v desire voltage.

4. Conclusion and Future Work

This paper presents a new implementation approach for PV tracking algorithm developed with both Proteus and MikroC software. It consists of mainly two parts: the first part is building a PV solar device in Proteus, which is new and has been proven by comparing the IV and PV characteristics' outcomes and the results from the MSX_60 datasheet. The second part is building the proposed algorithm in MikroC then using this PV to implement a PI controller to maintain the output voltage of the step-down converter constant during different weather conditions with the ability to modify the desired output voltage. Designing and implementing the discrete control tracking algorithm resulted in compatible system capable of working with the PIC18F4580 microcontroller from scratch. The validity of the proposed PV tracking technique has been proved with a perfect response time, and the results have been discussed in detail. It is possible to simulate a PV system with a bare current source representing the I_{ph}, and some blocks to emulate the Shockley diode equation and two resistances. This method allows the user to simulate various PV modules in platforms that don't support the PV cell. Simulink part showed a great potential to change temperature and irradiance at any time while running the program. In addition to that, by testing the proposed module with a voltage tracking algorithm, the system showed perfect response concerning temperature and irradiation changes. The presented simulator is composed of: building the PV panel model and testing it, designing DC-DC step-down converter with its accessories to trigger the switching mode, a voltage sensor to feed the voltage back into the proposed algorithm, an LCD screen, a PIC18F4580 microcontroller, a keypad for opting and modifying the desired input voltage, and implementing various mapping processes between adjacent inconsistent parts. This work would have a crucial role for researchers to simulate other panels in different circuit platforms, and to simplify the implementation of a wide range of applications and algorithms related to PV connection with many electrical applications. To reach the optimum design points, it is recommended to use some MCU that supports high bit resolution and use the transfer function provided in the literature of buck converter fed from PV cell. This transfer function describes precisely the relationship between the duty cycle and the output voltage of the load. This proposed work includes:

1. Using the C2d MATLAB function to convert the transfer function domain from the continuous to the discrete one with a predefined sampling time, depending on the coding algorithm and the designing requirements.
2. Importing the discrete transfer function with a close loop via the help of the MATLAB tuning tool in MATLAB Simulink to obtain the optimum PI parameters.
3. Using the same proposed tracking algorithm with the upgrading PI parameter would push the system to be more stable and to optimize the tracking path.

It is also possible to use platforms such as LabVIEW to help the user to reach the optimum PI parameter with the use of system identification. In this way, the researcher would be able to overcome

the analytical barriers associated with the assumptions in deriving the transfer function, such as omitting and approximating processes.

Statement of Conflict of Interest

Authors have declared no conflict of interest

Author Contributions

Writing—original draft preparation and software done by Mustafa HASAN; project administration, supervision, writing -review and editing done by Serra ALTINOLUK.

Nomenclatures

E_g :is the band gap energy of the semiconductor

G: the surface irradiance of the cell

G_{STC}: the irradiance under STC (=1000 W/m2)

$I_{s(STC)}$: the nominal saturation current;

$I_{sc(STC)}$: the short circuit current per cell at T_{STC}

K_B : the Boltzmann's constant;

K_i :the temperature coefficient of short circuit current

K_v : the temperature coefficient of open-circuit voltage

n: the diode ideality factor; STC is standard test conditions (T_{STC} = 25C)

T: the absolute temperature in K

I_{ph} : the light generated current

I_s : the saturation or leakage current of the diode

N_s: the number of cells in series for a PV module

N_p : the number of parallel modules

V_{OC}: the open-circuit voltage

R_s : series resistances of the solar cell

R_{sh} : parallel resistances of the solar cell

I_D: diode current or dark current.

Abbreviations

PWM: Pulse with Modulation

STC: Standard Test Conditions

TF: Transfer Function

LCD: Liquid Crystal Display

CCP: Capture/Compare/PWM

ADC: Analog Digital Converting

TMR0L: Timer0 Register Low Byte

TMR0H: Timer0 Register High Byte

T0CON: Timer0 control Register Byte

References

Akcan E., Kuncan M., Minaz MR. Modeling and simulation of 30 kw grid-connected photovoltaic system with PVsyst software. European Journal of Science and Technology 2020; 18: 248-261.

Ayim Otu B., Kuncan M., Horoz S. Research on renewable energy (solar) in Ghana. International Science and Engineering Symposium, 2019, Siirt, Turkey.

Bulut N., Kuncan M., Horoz S. Usage areas of solar energy in Turkey and solar energy potential in Siirt. Ahtamara 1st International Multidisciplinary Studies Congress Proceedings Book, August 2018, 1315-1319:,Van,Turkey.

Chalh A., El Hammoumi A., Motahhir S., El Ghzizal A., Subramaniam U., Derouich A. Trusted simulation using proteus model for a PV system: Test case of an improved HC MPPT algorithm. Energies 2020; 13(8): 1943.

Çiftçi S., Solak M., Kuncan M. Powered by the sun: designing and analyzing technical and economic aspects of a school sustained by photovoltaics. Journal of Mechatronics and Artificial Intelligence in Engineering 2020; 1(1): 21-32.

Doubabi H., Chennani M., Essounbouli N. Modeling and design of synchronous buck converter for solar-powered refrigerator. Proceedings of 2017 International Renewable and Sustainable Energy Conference (IRSEC), 4-7 December 2017,1-5:,Tangier, Morocco.

Erdoğan Y., Dinçler T., Kuncan M., Ertunç HM. High efficiency maximum power point tracker (MPPT) design for solar panels. Turkish Automatic Control Meeting, TOK, 2014; 1055-1060.

El Tayyan Ahmed A. A simple method to extract the parameters of the single-diode model of a PV system. Turkish Journal of Physics 2013; 37(1): 121-131.

Ergin Şahin M. Photovoltaic powered electrolysis converter system with maximum power point tracking control. International Journal of Hydrogen Energy 2020; 45(16): 9293-9304.

Geethanjali MN., Sidram MH. Performance evaluation and hardware implementation of MPPT based photovoltaic system using DC-DC converters. Proceedings of 2017 IEEE International Conference on Technological Advancements in Power and Energy: Exploring Energy Solutions for an Intelligent Power Grid (TAP Energy), 21-23 December 2017, 1–6:, Kollam, India.

Ghani ZA., Kamit K., Zeain MY., Zakaria Z., Azidin FA., Hadi NAA., Isira ASM., Othman H., Lago H. Development of a dc to dc buck converter for photovoltaic application utilizing peripheral interface controller. ARPN Journal of Engineering and Applied Sciences 2019, 14(7): 1317-1324.

Kandilli İ., Minaz MR., Kuncan M., Kuncan F. Design of cooling and heating system in cars with solar energy. International Conference on Multidisciplinary Science Engineering and Technology (IMESET'17) ,October 2017, 365-370:, Bitlis, Turkey.

Loba TH., Salim KM. Design and implementation of a micro-inverter for single PV panel based solar home system. In 2013 International Conference on Informatics, Electronics and Vision (ICIEV), 17-18 May 2013, 1-5:, Dhaka, Bangladesh.

Luque A., Hegedus S. Handbook of photovoltaic science and engineering. John Wiley & Sons; 2011.

Microchip. PIC18F2480/2580/4480/4580 Datasheet. Microchip 2007.

Motahhir S., Chalh A., Ghzizal A., Sebti S., Derouich A. Modeling of photovoltaic panel by using proteus. Journal of Engineering Science and Technology Review 2017; 10(2): 8-13.

Motahhir S., Chalh A., El Ghzizal A., Derouich A. Development of a low-cost PV system using an improved INC algorithm and a PV panel Proteus model. Journal of Cleaner Production 2018; 204: 355–365. https://doi.org/10.1016/j.jclepro.2018.08.246

Motahhr S., El Ghzizal A., Sebti S., Derouich A. Une ressource pédagogique pour l'enseignement par simulation : cas des panneaux photovoltaïques. Int Work Pedagog Approaches E-Learning 2015.

Mustafa RJ., Gomaa MR., Al-Dhaifallah M., Rezk H. Environmental impacts on the performance of solar photovoltaic systems. Sustain 2020; 12(2): 608.

Orioli A. An accurate one-diode model suited to represent the current-voltage characteristics of crystalline and thin-film photovoltaic modules. Renewable Energy 2020; 145: 725-743.

Pal D., Koniki H., Bajpai P. Central and micro inverters for solar photovoltaic integration in AC grid. In2016 National Power Systems Conference (NPSC), 19-21 Dec 2016, 1-6:, Bhubaneswar, India.

Rashid MH. Power electronics handbook. Butterworth-Heinemann; 2017.

Salman S., Ai X., Wu Z. Design of a P-&-O algorithm based MPPT charge controller for a stand-alone 200W PV system. Protection and Control of Modern Power Systems 2018; 3(1): 1-8.

Suroso Winasis, P., Purnama ID. Design of 1 kW buck-boost chopper with pi control for photovoltaic power conversion. IOP Conference Series: Materials Science and Engineering, 1 December 2020; 982(1). https://doi.org/10.1088/1757-899X/982/1/012022

Wang Y., Kamari ML., Haghighat S., Ngo PT. Electrical and thermal analyses of solar PV module by considering realistic working conditions. Journal of Thermal Analysis & Calorimetry 2021; 144(5): 1925-1934.

Yaqoob SJ., Obed AA. Modeling, simulation and implementation of PV system by proteus based on two-diode model. Journal of Techniques 2019; 1(1): 39-51.

Zekry A., Shaker A., Salem M. Solar cells and arrays: principles, analysis, and design. Advances in Renewable Energies and Power Technologies 2018: 3-56.

Zhou Z., Macaulay J. An emulated pv source based on an unilluminated solar panel and dc power supply. Energies 2017; 10(12): 2075.